# Improving Flux Pinning at High Fields in Intermetallic Superconductors: Clues From $MgB_2$ and $MgCNi_3$

Lance Cooley, Xueyan Song, and David Larbalestier

***Abstract*—We discuss flux pinning and nanostructural analyzes of two intermetallic superconductors that exhibit substantial deviations from the usual flux-shear behavior. Kramer plots for a $MgB_2$ thin film, which contained a substantial fraction of MgO nanoprecipitates, show an additional component that is attributed to core pinning by the precipitates. Also, polycrystalline $MgCNi_3$ displays a crossover from flux-shear to core pinning behavior as the temperature is reduced. At the same time, the flux line core diameter becomes comparable to the length scales of nanoprecipitates found by high-resolution electron microscopy. Thus, both experiments suggest that flux shear, and its low-field pinning characteristic, can be exceeded by incorporating nanoprecipitates in an intermetallic superconductor. However, too many precipitates within the grain boundaries can block uniform current flow between grains.**

***Index Terms*—Critical current density, flux pinning, intermetallic superconductors, magnesium diboride.**

## I. Introduction

GRAIN boundaries are the primary flux-pinning centers in most intermetallic superconductors. Since the average grain size $D$ is usually many times the flux-lattice constant $a_0$ even at moderate fields, the individual regions where flux lines intersect grain boundaries are widely separated. For example, in state-of-the-art $Nb_3Sn$ composites $D$ is $\sim$150 nm, slightly more than $10a_0$ at 12 T field. In this limit, the critical current is reached when the flux lattice deforms and eventually flows, which is governed by the shear modulus [1]. This produces a bulk flux pinning force $F_p(H) = \mu_0 H \cdot J_c(H)$ with a characteristic field dependence proportional to $h^{1/2}(1-h)^2$[2], where $h$ is the reduced field $H/H*$ and $H*$ is the irreversibility field. An algebraic transformation gives the so-called Kramer function $J_c^{1/2}H^{1/4}$, which decreases linearly with field (as in a "Kramer plot").

Linear Kramer plots are common for $MgB_2$[3]. Thus, flux shear may be the dominant pinning mechanism. An important feature of the flux-shear pinning mechanism is the low-field peak of the $F_p(H)$ curve, at about $0.2H^*$. This is obviously not desirable for high-field applications at $0.5H^*$ or higher. Recent experiments [4], [5] suggest that more desirable $F_p(H)$ curves can be obtained if $D$ is comparable to $a_0$, although benefits to pinning came at the expense of the critical temperature and upper critical field.

Manuscript received August 5, 2002. This work was supported in part by the U.S. Department of Energy and in party by the U.S. National Science Foundation through the MRSEC on Nanostructural Materials and Interfaces.

The authors are with the Applied Superconductivity Center, University of Wisconsin, Madison, WI 53706 USA ( e-mail: ldcooley@facstaff.wisc.edu).

Digital Object Identifier 10.1109/TASC.2003.812225

In this paper, we analyze the flux-pinning properties and nanostructures of two experiments that appear to break out of the limitations imposed by flux shear. In the first example, we analyze $MgB_2$ thin films made by pulsed laser deposition, which have $\sim$ 5 nm grains and $\sim$20% of MgO precipitates also with $\sim$5 nm size. The added core pinning by the MgO precipitates improves pinning at high field and at low temperature, when the superconducting coherence length is comparable to the precipitate dimensions. In the second example, we analyze a polycrystalline $MgCNi_3$ superconductor, which contains a nanoscale distribution of precipitates within the grains. Very strong pinning by these precipitates is found at low temperature, producing a $F_p(H)$ curve with a peak at $0.5H^*$, similar to that of Nb47wt.%Ti. Both of these experiments suggest that improved flux pinning can be obtained by incorporating nanoprecipitates in intermetallic superconductors.

## II. $MgB_2$ Thin Films: Core Pinning by Intergranular Nanoprecipitates in a Superconducting Matrix

In this section we discuss in more detail the magnetization analyzes of "film 2" from a series of $MgB_2$ thin films reported in [6]. A key feature of this film is its high $H^*$ due to alloying with oxygen, as indicated by slight shifts of the (001) and (002) x-ray diffraction peaks. Extensive x-ray diffraction characterization showed that the $MgB_2$ grains are very small, 5 to 7 nm, and are aligned with the c-axis perpendicular to the substrate but randomly in the substrate plane (fiber texture). These analyzes also suggested that the film contained $\sim$20% of MgO precipitates. The small grain size was confirmed by transmission electron microscopy [6], [7], which also revealed that the MgO precipitates had $\sim$5 nm size, as shown in Fig. 1(a).

Kramer plots derived from the magnetization data for this film are shown in Fig. 1(b). These plots are not linear at low fields and below 15 K, but instead curve downward with increasing field until abruptly changing to linear behavior at a high field $H_{\rm Lin}$. For instance, $H_{\rm Lin}$ is approximately 13 T for the 4.2 K curve, as indicated on the plot. The Kramer curves above 15 K lack any transition and have the more usual linear decrease with field. An interesting possibility is that the downward curvature below 15 K and $H_{\rm Lin}$ is due to additional core pinning by the MgO precipitates. Since $F_p(H) \propto h(1-h)$ for core pinning by small precipitates [8], the Kramer function would be proportional to $h^{1/4}(1-h)^{1/2}$ and would be approximately parabolic at high field. To explore this possibility further, a linear fit to the measured Kramer curve above $H_{\rm Lin}$ was subtracted from the $F_p(H)$ data at 4.2, 10, and 15 K, and the result is plotted in Fig. 1(c). When normalized, these curves have shapes very close to $h(1-h)$.

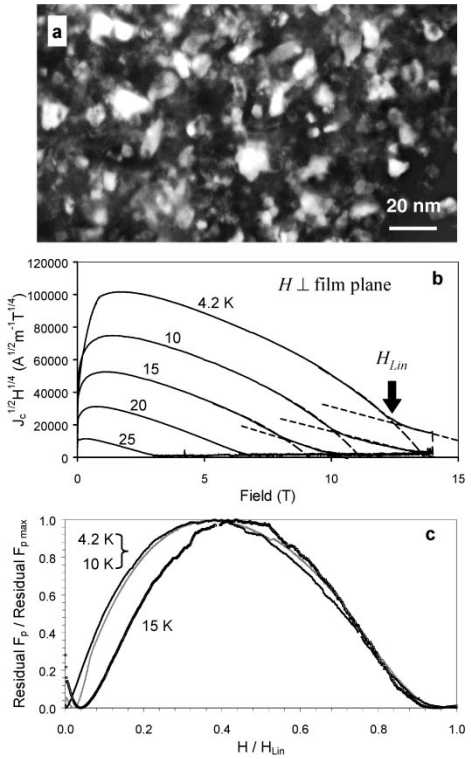


Fig. 1. (a) Transmission electron micrograph of the $MgB_2$ film 2 from [6]. Only some of the grains are brightly diffracting, showing the grain size. (b) Kramer plots at 4.2 to 25 K for this film. Dashed and dotted lines are guides to the eye. The falloff near zero field is an artifact of the reversal of the magnetization loop from a saturated critical state. (c) Bulk pinning-force curves derived from magnetization data, after subtracting a linear Kramer function fit to high field data in (b), indicated by the dotted lines.

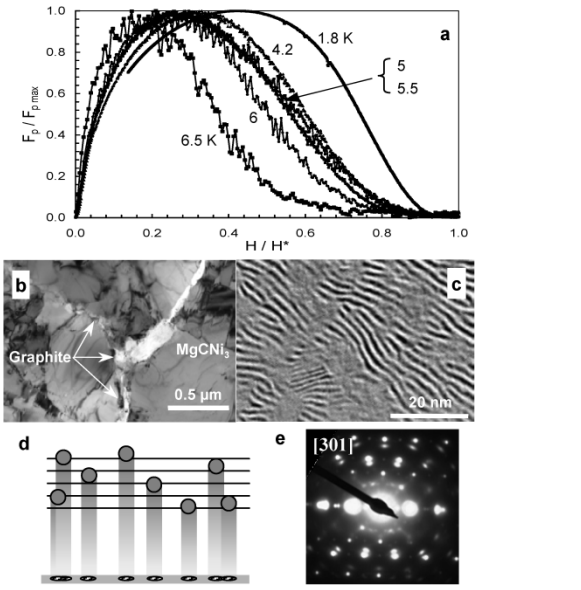


Fig. 2. (a) Reduced bulk pinning force curves for $MgCNi_3$, from [12]. (b) Transmission electron micrograph, showing a graphite layer between colonies of $MgCNi_3$ grains. (c) High-resolution TEM image taken along the [301] zone axis, showing Moiré fringe domains due to unidentified cubic precipitates. (d) A schematic of the fringe generation, indicating how the precipitate size corresponds with the observed domains. (e) Selected area diffraction pattern for the same zone axis as in (c). Satellite spots next to the main spots indicate that the precipitate has a lattice parameter 25% larger than the parent $MgCNi_3$ phase and has cube-on-cube alignment.

We admit that we do not fully understand why the Kramer plots abruptly change at $H_{\rm Lin}(T)$ and core pinning apparently disappears with increasing field. Since this $MgB_2$ film is among the first ones made, one possibility is that the film is not homogeneous but is instead divided into 2 different superconducting regions with 2 different pinning mechanisms. In one region, core pinning is dominant, perhaps due to the presence of MgO precipitates. This region apparently has a critical temperature between 15 and 20 K, and may have $H^*_\perp(T) \approx H_{\rm Lin}(T)$. In the other region, flux-shear is dominant, perhaps due to a lack of precipitates. This region has the higher critical temperature and $H^*(T)$ reported previously [6], [9].

Nonetheless, we believe the presence of a large fraction of MgO precipitates and the observation of Kramer curves consistent with core pinning are related. Since the precipitates are $\sim$5 nm in size, they are slightly smaller than the flux line core diameter at 0 K, $2\xi(0) \approx 8$ nm [9], and thus have nearly ideal size for core pinning. The precipitates are also embedded in a matrix of nanoscale $MgB_2$ grains, which may function as a homogeneous medium since grain boundaries are not weak links [3]. Perhaps the situation is similar to that in Nb–Ti alloys, where strong pinning by precipitates dominates the background pinning of grain boundaries [10].

## III. $MgCNi_3$: Core Pinning by Intragranular Nanoprecipitates

$MgCNi_3$ is another superconductor discovered in 2001, with a $T_c$ of $\sim$8 K in specimens prepared with a substantial excess of carbon [11]. In this section we summarize our combined electromagnetic and nanostructural analyzes of a sample prepared with overall composition $MgC_{1.5}Ni_3$, $T_c$ of 7.2 K, and $\mu_0 H_{c2}(0)$ of 12.4 T [12]. Magnetization measurements showed that the sample has unusual flux pinning properties for an intermetallic superconductor, shown in Fig. 2(a). While flux shear is indicated at 6.5 K, $F_p(h)$ changes smoothly with decreasing temperature, and at 1.8 K it has the curve shape expected for core pinning. Moreover, the smooth evolution of pinning-force curves with decreasing temperature is very similar to that seen in Nb–Ti alloys [10], suggesting a dense nanostructure of pinning centers.

Electron microscopy analyzes, summarized in Fig. 2(b), showed that the microstructure consists of colonies of $MgCNi_3$ grains surrounded by a network of graphite. The graphite is believed to subdivide the magnetization current loops to $\sim$10 $\mu$m diameter. Higher magnification showed that each colony contains 100 to 300 nm grains. Higher resolution images of the grain interiors reveal a system of Moiré fringes, Fig. 2(c), indicative of fine precipitates [13]. The fringe domain size suggests that the precipitates have $\sim$5 nm size, as the sketch in Fig. 2(d) illustrates. Diffraction patterns, such as the one shown in Fig. 2(e), indicate that the precipitates have cubic symmetry and a lattice parameter that is 25% larger than that of the $MgCNi_3$. Thus, the precipitates have a 5-on-4 commensuration with the parent lattice. So far, we have not been able to identify the precipitates.

Since the precipitate diameters are comparable to the flux line core size at 0 K, they are strong core pinning sites and capable of producing the characteristic $h(1-h)$ curve. At higher temperature, the increase of $\xi(T)$ causes the flux line cores to expand above the length scale of the nanostructure, which decreases

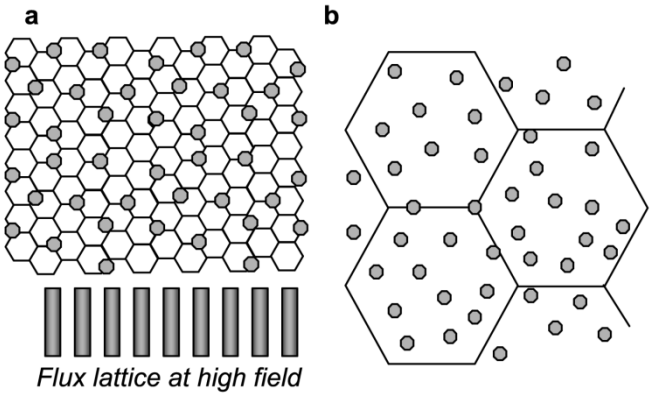


Fig. 3. (a) Schematic of core pinning in the $MgB_2$ thin film. White hexagons represent superconducting grains, while gray circles represent nonsuperconducting precipitates. Below the sketch is indicated the corresponding flux line size and separation at high field. (b) Schematic of core pinning in $MgCNi_3$. White hexagons again represent superconducting grains and gray circles precipitates. The sketch is to scale with (a).

their effectiveness as pinning centers. As in Nb–Ti, the background pinning by grain boundaries is present at all temperatures, and grain boundaries may dominate near $T_c$. This explains why the peak of $F_p(h)$ shifts toward lower field with increasing temperature, from a curve consistent with core pinning to one consistent with flux shear.

## IV. Discussion

While the particular physics associated with the flux shear pinning mechanism has been debated for a long time, the most recent work suggests that the flux line lattice (FLL) is plastically deformed by the Lorentz and pinning forces [14]. In this case, dislocations separate elastically correlated domains of flux lines. At the critical current, such correlated flux domains might slide past each other along dislocated domain walls. In this disordered regime, the shear modulus for dislocation motion defines the critical current density. Breaking out of this limit therefore requires destruction of flux-lattice order, in favor of the single fluxon pinning limit believed to be valid for very dense arrangements of pinning centers such as in Nb–Ti. In this case, elementary pinning interactions can be summed directly. In principle, this limit occurs if strong pinning sites are arranged over length scales comparable to $a_0$[15].

The two scenarios for exceeding flux-shear limits at high fields described above are summarized in the diagrams in Fig. 3. In Fig. 3(a), a nanoscale mixture of superconducting grains and precipitates is considered. The nanoscale granular matrix should be transparent to current flow in this case, and it should be relatively free from blocking layers or other quasicontinuous interfaces. Fig. 3(a) is suggestive of an artificial mixture of nanoparticles that are sintered together. In Fig. 3(b), nanoprecipitates or similar point pinning sites are added inside the grains. In this case, other precipitation modes, such as grain-boundary films or triple-point precipitation, can obstruct current flow across the boundaries. Fig. 3(b) is suggestive of a continuous metastable solid solution, from which precipitates have been formed. Thus, while the two scanarios are conceptually identical, the particular obstacles and practical fabrication routes may be quite different.

In both $MgB_2$ and $MgCNi_3$, core pinning by small precipitates exceeds the pinning by grain boundaries at high field and low temperature, which is the field and temperature range of interest for magnet applications. This can be the result of either a stronger elementary core-pinning force or a higher number of core pinning interactions, or both. While core pinning sites probably outnumber grain-boundary interactions in $MgCNi_3$, the very small grain size of the $MgB_2$ film suggests that pinning interactions with grain boundaries can occur with comparable frequency along the length of a flux line as interactions with MgO precipitates. We infer, therefore, that the elementary core-pinning interaction must be stronger than that of the grain boundaries. If the nonlocal Josephson treatment of grain boundaries is valid [16], the apparently weaker pinning strength of grain boundaries would be consistent with strong coupling, far above any weak link threshold. Our assumption, that the $MgB_2$ matrix functions as a homogeneous medium as far as core pinning is concerned, may thus be valid.

Moreover, since $D \approx a_0$ in the thin film experiment, it is curious why the background pinning by grain boundaries does not produce deviations from linear Kramer curves, as seen in $Nb_3Sn$ recently [4], [5]. Perhaps this is further evidence that grain boundaries are not as effective pinning centers in $MgB_2$ as they are in other intermetallic superconductors such as $Nb_3Sn$. Two key factors may be the rather long coherence length of $MgB_2$, $\xi(0) \geq 4$ nm, and the fact that $MgB_2$ so far appears to tolerate very limited variations from stoichiometry. These factors would subdue the effects of structural or chemical variations along grain boundaries that produce the pinning force [16], [17]. While this argument may be contradictory to the good pinning observed in many bulk samples, tapes and wires, recent microscopy work [7], [18], [19] suggests that MgO precipitates are common in $MgB_2$ samples.

Several experiments have attempted to produce nanostructures similar to the models in Fig. 3. Wang *et al.* [20] added $Y_2O_3$ nanoparticles to a mixture of Mg and B powders. This produced a somewhat unexpected distribution of $YB_4$ nanoprecipitates within $MgB_2$ grains, as in Fig. 3(b). However, larger nanoprecipitates formed network in the grain boundaries that partially closed off transport current. Thus, one potential obstacle against optimizing nanoprecipitate formation is favored precipitation in the grain boundaries. Nonetheless, the high critical current densities were inferred from magnetization measurements, which must be very high on the single grain scale. Dou *et al.* [21] explored a similar process using SiC nanoparticles, where although $Mg_2Si$ precipitates were formed, C alloyed with $MgB_2$ to produce poor superconducting properties. The wide range of stable borides and the extreme stability of MgO suggests very interesting flux-pinning structures can be obtained for various nanoparticle mixtures.

## V. Conclusions

We discussed flux pinning and nanostructural analyzes of two intermetallic superconductors that exhibit substantial deviations from the usual flux-shear behavior. In the first experiment, an $MgB_2$ thin film that contained a substantial fraction of nanoscale MgO precipitates was considered. Kramer

plots contained an additional component that was attributed to core pinning by the precipitates, leading us to conclude that one scenario for exceeding flux-shear limits is to embed nonsuperconducting nanoprecipitates in a matrix of nanoscale superconducting grains. In the second experiment, $MgCNi_3$ displayed a crossover from flux-shear to core pinning behavior as the temperature was reduced. At the same time, the flux line core diameter became comparable to the length scales of nanoprecipitates found by high-resolution electron microscopy. This experiment suggested that a second scenario for exceeding flux shear is to incorporate nanoprecipitates inside the grains of an intermetallic superconductor. However, in this latter configuration precipitates within the grain boundaries can block uniform current flow between grains.

## ACKNOWLEDGMENT

The authors wish to thank E. Hellstrom, C.-B. Eom, X. Song, S. Patnaik, V. Braccini, B. Senkowicz, P. Lee, and R. Cava for scientific discussions. The $MgB_2$ thin film was provided by C.-B. Eom, University of Wisconsin, and the $MgCNi_3$ sample was provided by R. Cava, Princeton University.

## REFERENCES

[1] E. J. Kramer, "Scaling laws for flux pinning in hard superconductors," *J. Appl. Phys.*, vol. 44, pp. 1360–1370, 1973.

[2] A. Kahan, "Frank-Read source-activated flux shear in type-II superconductors," *Phys. Rev. B*, vol. 43, pp. 2678–2686, 1991.

[3] D. C. Larbalestier *et al.*, "Strongly linked current flow in polycrystalline forms of the superconductor $MgB_2$," *Nature (London)*, vol. 410, pp. 186–189, 2001.

[4] L. D. Cooley and P. J. Lee, "Shift of the flux-pinning force curve in $Nb_3Sn$ thin films with very fine grain size," *IEEE Trans. Appl. Supercond.*, vol. 11, pp. 3820–3823, 2001.

[5] L. D. Cooley, P. J. Lee, and D. C. Larbalestier, "Changes in flux pinning curve shape for flux-line separations comparable to grain size in $Nb_3Sn$ wires," *Adv. Cryo. Eng. (Materials)*, vol. 48B, pp. 925–932, 2002.

[6] C. B. Eom *et al.*, "High critical current density and enhanced irreversibility field in $MgB_2$ thin films," *Nature (London)*, vol. 411, pp. 558–560, 2001.

[7] X. Song *et al.*, "Anisotropic grain morphology, crystallographic texture and their implications for flux pinning mechanisms in $MgB_2$ pellets, filaments and thin films," *Supercond. Sci. Technol.*, vol. 15, pp. 511–518, 2002.

[8] A. M. Campbell and J. E. Evetts, "Flux vortices and transport currents in type-II superconductors," *Adv. Phys.*, vol. 21, pp. 199–428, 1972.

[9] S. Patnaik *et al.*, "Electronic anisotropy, magnetic field-temperature phase diagram and their dependence on resistivity in $c$-axis oriented $MgB_2$ thin films," *Supercond. Sci. Technol.*, vol. 14, pp. 315–319, 2001.

[10] C. Meingast and D. C. Larbalestier, "Quantitative description of a very high critical current density Nb–Ti superconductor during its final optimization strain. II. Flux pinning mechanisms," *J. Appl. Phys.*, vol. 66, pp. 5971–5983, 1989.

[11] T. He *et al.*, "Superconductivity in the nonoxide perovskite $MgCNi_3$," *Nature (London)*, vol. 411, pp. 54–56, 2001.

[12] L. D. Cooley, X. Song, J. Jiang, D. C. Larbalestier, T. He, K. A. Regan, and R. J. Cava, "Core pinning by intragranular nanoprecipitates in polycrystalline $MgCNi_3$," Phys. Rev. B, vol. 66, to be published.

[13] W. Kesternich, "Materials problem solving with the transmission electron microscope," in *Symposium. Mater. Res. Soc*, Pittsburgh, PA, 1986, p. 229.

[14] E. H. Brandt, "Elastic and plastic properties of the flux-line lattice in type-II superconductors," *Phys. Rev. B*, pp. 6514–17, 1986.

[15] G. P. van der Meij and P. H. Kes, "Effective volume of voids for flux pinning in superconductors," *Phys Rev. B*, vol. 29, pp. 6233–43, 1984.

[16] A. Gurevich and L. D. Cooley, "Anisotropic flux pinning in a network of planar defects," *Phys Rev. B*, vol. 50, pp. 13 563–76, 1984.

[17] A. Gurevich and E. A. Pashitskii, "Enhancement of superconductivity at structural defects in high-temperature superconductors," *Phys Rev. B*, vol. 56, pp. 6213–25, 1997.

[18] X. Z. Liao, A. C. Serquis, Y. T. Zhu, J. Y. Huang, D. E. Peterson, F. M. Mueller, and H. F. Xu, "Controlling flux pinning precipitates during $MgB_2$ synthesis," *Appl. Phys. Lett.*, vol. 80, pp. 4398–4400, 2002.

[19] R. F. Klie, J. C. Idrobo, N. D. Browning, A. Serquis, Y. T. Zhu, X. Z. Liao, and F. M. Mueller, "Observation of coherent oxide precipitates in polycrystalline $MgB_2$," *Appl. Phys. Lett.*, vol. 80, pp. 3970–72, 2002.

[20] J. Wang *et al.*, "High critical current censity and improved irreversibility field in bulk $MgB_2$ made by a scaleable, nanoparticle addition route," Appl. Phys. Lett., 2002, to be published.

[21] S. X. Dou, A. V. Pan, S. Zhou, M. Ionescu, H. K. Liu, and P. R. Munroe, "Substitution Induced Pinning in $MgB_2$ Superconductor Doped with SiC Nano-Particles,", cond-mat/0 206 444.